JOURNAL OF THEORETICAL
AND APPLIED MECHANICS
4, **37**, 1999

ON INTERACTION BETWEEN DAMAGE GROWTH AND MATERIAL STIFFNESS IN 3D STRUCTURES

PIOTR MIKA

Institute of Computer Methods in Civil Engineering, Cracow University of Technology
e-mail: plmika@kinga.cyf-kr.edu.pl

Deterioration of material properties; such as, rupture toughness, strength, and rigidity as well as lifetime reductions are modelled by a symmetric second order damage tensor introduced into the constitutive description, when employing the theory of tensor function representations. The growth of damage and state of failure are described by a one parameter model of damage evolution and a three parameter failure criterion. The constitutive description for different modes of failure front propagation is of particular interest in this study. The comparison between solutions obtained by means of two different physical models; i.e., the linear elastic and linear elastic with damages ones, respectively, has been presented. In both cases the stress redistribution due to geometrical changes of the structure induced by the crack propagation has been considered. Numerical calculations have been made employing the ABAQUS programme, Runge-Kutta procedures for integration of the evolution equations, standard methods of matrix division in LU decomposition and Gauss method for solving the set of linear equations.

Key words: damage mechanics, evolution equation, material stiffness

1. Introduction

Theoretical estimation of the first crack instants and time intervals for carrying capacity deformation is one of the crucial research issues in a design process of viscoelastic solid structures. Very intensive development of Continuum Damage Mechanics (CDM) in recent twenty years has not brought about an effective model complying with the solid thermodynamics requirements. There should be some possibilities of description of the model behaviour: anisotropic

damage development, one-sideness of nodes in crack zones and complex non-proportional loads, (cf Chaboche, 1990). Therefore application of the model to modern engineering structures is limited.

The relations between the methods of statistical physics associated with the structure of the material and the possibility to indicate a common basis of continuum constitutive theory in terms of self-consistent and effective field models were analysed by Krajcinovic (1996). The basic concepts of damage mechanics were considered with stochastic models used on atomic scales, micromechanical models on macroscopic scales, and continuum models on macroscales, Krajcinovic et al. (1994), Krajcinovic (1996).

The nowadays tendencies of damage mechanics reflect in a tensor model is used in this paper. In this model the tensorial damage measure derived by Murakami and Ohno (1981) is applied. The damage evolution equation by Litewka and Hult (1989) according to Vakulenko and Kaczanov idea (1971) with later amendments by Murakami and Ohno (1981), Murakami and Sanomura (1985) has been adopted. The criterion of failure in a material with decreasing strength in its evolution process specifies the energetic isotropic medium with damages, defining a three-parameter surface of critical states calibrated experimentally in two uniaxial tensions in perpendicular directions and biaxial tension. Physical properties of the material are modelled using the constitutive coupling of damage tensor with the stress and strain tensors invented by Litewka (1985).

The material orthotropy issues from the assumed symmetry of the damage tensor. The principal values of the damage tensor introduced into the physical model are used for modification of stiffness variable in time.

Professional computer codes, e.g. ABAQUS and high capacity computers allowed for application of complex mathematical models; e.g., implementation of tensorial measures, coupling of damage with constitutive description and integrating the evolution equations. Nevertheless, in some calculations presented in other papers one can find that scalar measures are applied to the damage analysis in the cases where sufficient agreement between the experimental and calculated results can be achieved. Calculations of composite laminated plates and shells provide an example of such an analysis, e.g. Saleeb and Wilt (1993). The law of evolution was written there in terms of the isochronous failure/damage function. The constitutive equations for the coupled viscoplastic damage response were used in conjunction with a finite element model. The authors presented a development of the general computation framework for numerical implementation using the Euler fully-implicit integration method.

The application of tensorial measures to the analysis of structure elements

was given by Murakami and Hayakawa (1997). The constitutive and damage evolution equations of elastic-plastic material subject to damage were developed on the basis of irreversible thermodynamic theory of constitutive equations. The resulting equations could describe the anisotropic change in the elastic properties of spheroidal graphite cast iron due to damage.

A two-dimensional self-consistent micromechanical tensorial damage model was presented for microcrack-weakened brittle solids by Ju (1991). The stability criteria of fracture mechanics together with microstructural geometry were employed in description of the microcrack evolution. The proposed numerical algorithm was tested uniaxial tension and compression and biaxial compression/tension, respectively.

An alternative approach to the continuum damage modelling, cf Vakulenko and Kachanov (1971), consists in the micromechanical model with averaging procedures and homogenisation for composites with fibrous metal applied by Voyiadjis and Park (1995). The damage was represented by a fourth-order overall damage tensor. The damage evolution equation was introduced assuming that the energy amounts dissipated due to plasticity and damage, respectively, were independent of each other. As an example, an analysis of the layered composite under uniaxial load taking into considerations the fibre direction is presented. A very good correlation was found between the numerical results obtained by using the proposed theory and the experimental results.

The paper presents continuation of the investigations presented by Białkiewicz and Kuna (1996), Białkiewicz and Mika (1995) but including damage into the constitutive equation with the stress and strain coupling. Białkiewicz and Kuna (1996) focused on the dependence of the Mindlin-Reissner plate load distribution on the damage mechanism and concentrated on the effect of elastic strain energy density and stresses on the mode of rupture front propagation. The stress redistribution and damage evolution in plates caused by the width of damage front and generated by changes in geometry were analysed by Białkiewicz and Mika (1995). Different physical properties of the plate cross-section were modelled by means of a layered finite element.

Because of high non-linearity introduced into the model by the evolution equation, failure criterion and constitutive coupling, it is difficult and in some cases even impossible to predict the crack propagation mechanism.

The numerical analysis proposed in the paper aims at investigation into the effect of material stiffness reduction in the constitutive equations on evolution of the damage process. The effect of changes in the plate stiffness on the damage growth rate and the first crack time relative to the structure lifetime as well as prediction of a possible damage mechanism responsible for initia-

tion and growth of damage zones are analysed. The solution is illustrated by investigation into the damage tensor eigenvalue function variability along the orthotropy directions, the resulting stress redistribution and the plate deflection growth.

The ABAQUS (cf Hibbitt et al., 1997) program has been used in calculations. The mathematical model of the constitutive equation, damage evolution and failure criterion has been defined in the user material procedure (UMAT). The first order eight-nodal solid elements with reduced integration were used. Due to the requirements of the UMAT procedure defining the mathematical model, the Jacobian will be generated through lower triangular and upper triangular (LU) matrix decomposition procedures (cf Press et al., 1992). Integration of the damage evolution equation has been performed by application of the Runge-Kutta standard procedures (cf Press et al., 1992). To solve the sets of algebraic equations determining the failure criterion parameters – at each discrete integral step – the Gauss method has been applied.

2. Mathematical model

The constitutive equation of the linear elastic medium with damage is assumed as an isotropic tensor function, in which the strain tensor $\boldsymbol{\varepsilon}$ is related to the stress and damage tensors, denoted as $\boldsymbol{\sigma}$ and $\mathbf{D}$, respectively (cf Litewka, 1985)

$$\boldsymbol{\varepsilon} = F(\boldsymbol{\sigma}, \mathbf{D}) \tag{2.1}$$

Basing on the theory of tensor function representations and the stress-strain law of elasticity, Eq (2.1) is accepted as in the case of linear elastic material in which variable in time stiffness depends on the damage increase level

$$\varepsilon_{ij} = A_{ijkl}(D_{mn})\sigma_{kl} \tag{2.2}$$

and the constitutive compliance matrix $\mathbf{A} = [A_{ijkl}]$ is a function of the damage tensor components

$$\begin{aligned} A_{ijkl} &= -\frac{\nu}{E}\delta_{ij}\delta kl + \frac{1+\nu}{2E}(\delta_{ik}\delta jl + \delta_{il}\delta jk) + \\ &+ \frac{D_1}{4E(1+D_1)}(\delta_{ik}D_{jl} + \delta jlD_{ik} + \delta_{il}D_{jk} + \delta jkD_{il}) \end{aligned} \tag{2.3}$$

where E and ν are the temperature-dependent Young modulus and Poisson ratio of the undamaged material. In order to derive the evolution equation

we use the tensor $\mathbf{\Omega}$ of principal values related to $\mathbf{D}$ by (cf Murakami and Sanomura, 1985)

$$\Omega_i = \frac{D_i}{1+D_i} \qquad i = 1,2,3 \tag{2.4}$$

The standards of ABAQUS programme require that Eq (2.2) be rewritten in a matrix form

$$\boldsymbol{\varepsilon} = \mathbf{K} \cdot \boldsymbol{\sigma} \tag{2.5}$$

where $\mathbf{K} = [K_{IJ}]$ and

$$\begin{aligned} \boldsymbol{\varepsilon}^{\top} &= [\varepsilon_{11}, \varepsilon_{22}, \varepsilon_{33}, \gamma_{12}, \gamma_{13}, \gamma_{23}] \\ \boldsymbol{\sigma}^{\top} &= [\sigma_{11}, \sigma_{22}, \sigma_{33}, \sigma_{12}, \sigma_{13}, \sigma_{23}] \end{aligned} \tag{2.6}$$

The two-dimensional stiffness matrix is generated by substituting for the suitable elements of the matrix $[A_{ijkl}]$ according to the scheme given in the table below

$$K_{IJ} = A_{ijkl} \tag{2.7}$$

and

I,J	1	2	3	4	5	6
i,k	1	2	3	2,3	1,3	1,2
j,l	1	2	3	3,2	3,1	2,1

e.g. $K_{24} = A_{2232}$.

Coordinates of the constitutive matrix $\mathbf{K}$ (see Eq (2.7))

$$\mathbf{K} = \frac{1}{E} \begin{bmatrix} \tilde{\mathbf{K}}_{11} & \tilde{\mathbf{K}}_{12} \\ \tilde{\mathbf{K}}_{12}^{\top} & \tilde{\mathbf{K}}_{22} \end{bmatrix}$$

are the submatrices

$$\begin{aligned} \tilde{\mathbf{K}}_{11} &= \begin{bmatrix} 1+\Omega_1 D_{11} & -\nu & -\nu \\ -\nu & 1+\Omega_1 D_{22} & -\nu \\ -\nu & -\nu & 1+\Omega_1 D_{33} \end{bmatrix} \\ \tilde{\mathbf{K}}_{12} &= \begin{bmatrix} \Omega_1 D_{12} & \Omega_1 D_{13} & 0 \\ \Omega_1 D_{12} & 0 & \Omega_1 D_{23} \\ 0 & \Omega_1 D_{13} & \Omega_1 D_{23} \end{bmatrix} \\ \tilde{\mathbf{K}}_{22} &= \begin{bmatrix} \tilde{\nu}+\Omega_1(D_{22}+D_{11}) & \Omega_1 D_{23} & \Omega_1 D_{13} \\ \Omega_1 D_{23} & \tilde{\nu}+\Omega_1(D_{11}+D_{33}) & \Omega_1 D_{12} \\ \Omega_1 D_{13} & \Omega_1 D_{12} & \tilde{\nu}+\Omega_1(D_{22}+D_{33}) \end{bmatrix} \end{aligned} \tag{2.8}$$

where $\tilde{\nu} = 2 + 2\nu$.

When computing the inverse constitutive matrix $\mathbf{K}^{-1}$ at each discrete integral step the decomposition procedure in lower and upper triangular matrices (LU procedure based on Ctout's algorithm, which assumes the suitable order for equation solving) has been applied. To solve the equilibrium equation the Newton-Raphson iteration procedure has been applied.

The time step is controlled by the numerical solution convergence and permissible at every iteration through principal values increase of the damage tensor in evolution equation integral procedure, cf Litewka and Hult (1989)

$$\partial_t \Omega_i = k(\boldsymbol{M}\boldsymbol{N}^{\top})^2 \sigma_i H(\sigma_i) \qquad i = 1,2,3 \tag{2.9}$$

where

$$\begin{aligned} \boldsymbol{M} &= \Big[\frac{1-2\nu}{6E}, \frac{1+\nu}{2E}, \frac{\Omega_1}{2E}\Big] \\ \boldsymbol{N} &= \Big[\operatorname{tr}^2\boldsymbol{\sigma},\ \operatorname{tr}\mathbf{S}^2,\ \operatorname{tr}(\boldsymbol{\sigma}^2\mathbf{D})\Big] \end{aligned} \tag{2.10}$$

where $\mathbf{S}$ is stress deviator.

The Heaviside function H involved in the evolution equation (2.9) eliminates the damage growth in the directions of compressive stresses σ_i, and k is the temperature dependent material constant of the evolution equation, cf Litewka and Hult (1989). The Runge-Kutta fourth order integral procedure has been used to integrate the damage evolution equation. The initial conditions will be formulated for the undamaged plate material $\Omega_i = D_i = 0$.

The vector of material constants $\boldsymbol{C} = [C_1, C_2, C_3]$ defines the actual hypersurface configuration of critical states, cf Litewka (1985)

$$\boldsymbol{C}\boldsymbol{R} - s_u^2 = 0 \tag{2.11}$$

where

$$\boldsymbol{R} = \frac{1}{s_1^2}\begin{bmatrix} (s_1+s_2+s_3)^2 \\ s_1^2+s_2^2+s_3^2-s_2s_1-s_3s_1-s_2s_3 \\ \Omega_1\Big(\dfrac{s_1r_1^2}{s_1-r_1\Omega_1}+\dfrac{s_2r_2^2}{s_1-r_2\Omega_1}+\dfrac{s_3r_3^2}{s_1-r_3\Omega_1}\Big) \end{bmatrix} \tag{2.12}$$

In the postulated failure criterion (2.11) the dimensionless stress magnitude has been applied

$$\begin{aligned} s_i &= \frac{\sigma_i}{\sigma_u} \qquad r_i = s_i H(s_i) \qquad i = 1,2,3 \\ s_u &= \frac{\sigma_u}{\sigma_1} \end{aligned} \tag{2.13}$$

where σ_u is time dependent ultimate strength of the undamaged material, and σ_1 is the maximal tensile stress.

The damage evolution has an effect on contraction of the hyper-surface (2.11) reducing the pre-critical state space. The components of vector $\boldsymbol{C}$ are determined at each discrete moment of numerical integration, as a result of application of Eq (2.11) to the three different states of stress: two cases of uniaxial tension in the perpendicular directions (coaxial with principal directions of the damage tensor) and biaxial tension in the same directions. In this paper the values of the two uniaxial and biaxial ultimate strengths of the damaged material have been assumed in the form related to the uniaxial ultimate tensile strength

$$\begin{aligned} \sigma_{1u} &= \sigma_{bu} = (1 - \Omega_1)\sigma_u \\ \sigma_{2u} &= (1 - \Omega_2)\sigma_u \end{aligned} \tag{2.14}$$

following the theoretical and experimental investigations carried out by Żuchowski (1986).

This procedure leads to the set of three algebraic equations to be solved with respect to the components of vector $\boldsymbol{C}$

$$\mathbf{U}\boldsymbol{C}^{\top} = \mathbf{I} \tag{2.15}$$

where

$$\mathbf{U} = \begin{bmatrix} (1-\Omega_1)^2 & \frac{2}{3}(1-\Omega_1)^2 & (1-\Omega_1)^2\Omega_1 \\ (1-\nu_2\Omega_1)^2 & \frac{2}{3}(1-\nu_2\Omega_1)^2 & (1-\nu_2\Omega_1)\nu_2\Omega_1 \\ 4(1-\Omega_1)^2 & \frac{2}{3}(1-\Omega_1)^2 & 2(1-\Omega_1)\Omega_1 \end{bmatrix} \tag{2.16}$$

The solution algorithm is based on calculation of the current stresses, strains and displacements, which depend on state of damage. The calculations have been performed using the standard finite element method (FEM) and the constitutive equation (2.5) introduced by the UMAT procedure. The user variables have been included in the procedure storing the current damage tensor values and a variable informing that there is a crack in a given element. By adopting solid 3D elements it is possible to use the UMAT procedure to analyse the beam and plate structures, e.g. Kuna and Mika (1996).

Since the boundary conditions can be defined only globally for finite elements (limitations of ABAQUS, ver. 5.4), the elements with reduced integration have been used. Moreover, this type of elements eliminates the "shear

locking" phenomenon, which appears in bending problems. To avoid the "hourglass stiffness", (cf Hughes, 1987), the plate cross-section has been divided into five layers of finite elements.

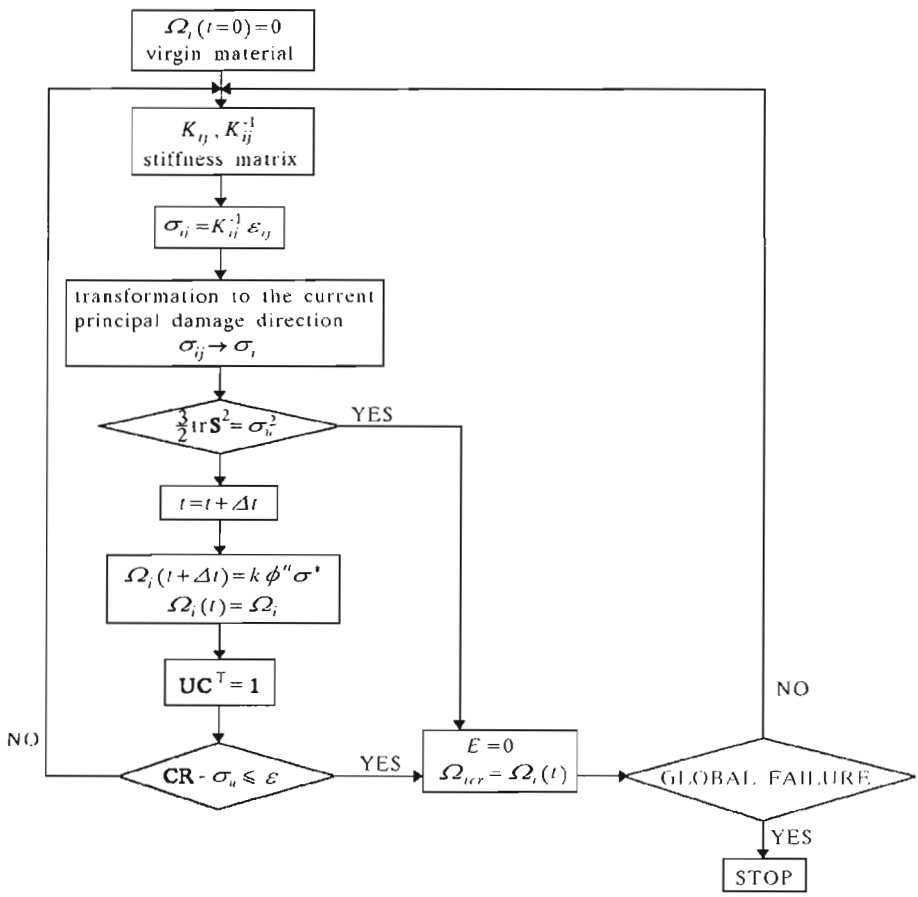

Fig. 1.

The block diagram of the UMAT procedure calculating the current field of stresses and the **K**-matrix components, is presented below.

At first, we find the elastic solution for a virgin material and then the damage evolution process starts. After transforming the damage and stress tensors to the damage principal directions, the failure criterion is checked at the beginning of each time increment. If the failure criterion in the element is satisfied, the material stiffness in the element is reduced to zero. The work presented by Hsiao, Fong and Gibbons showed that the zero modulus

approximation greatly facilitated application of the CDM modelling with no significant loss in accuracy, (cf Hsiao et al., 1997). Then the elastic compliance matrix has been updated according to the current state of damage.

The UMAT procedure also integrates the evolution equation on the basis of calculated stress values.

3. Numerical example

As a numerical example we consider a uniformly loaded square plate with the clamped edges, Fig.2a. Due to symmetry, we can consider only one quarter of the plate ABCDEFGH, Fig.2b, where ABFE and ADHE are the clamped planes, BCFG and CDGH are the symmetry planes, whereas the sought functions are symmetrical with respect to the ACGE plane. The square plate has been divided into the first order solid elements with reduced integration of $12 \times 12 \times 5$ in size. The elements are numbered in rows, starting from the bottom layer. The numbers in the figure denote the element numbers for which the history of the variables characteristic for the process will be shown.

In the numerical solution we use the following values for dimensionless parameters: Young modulus $\overline{E} = E/\sigma_u = 417$, Poisson ratio $\nu = 0.47$, $\overline{k} = k\sigma_u^3\tau = 82.1$, see Eq (2.9), where $\tau = 1\,\mathrm{h}$ is the unit time. The assumed parameters represent carbon steel at the temperature of 811 K (cf Białkiewicz and Mika, 1995), revealing the ultimate strength $\sigma_u = 288\,\mathrm{MPa}$. Also the dimensionless uniform load parallel to the external normal $\overline{q} = q/\sigma_u = 3.8 \cdot 10^{-2}$ and the dimensionless plate thickness $\overline{h} = h/a = 0.1$ where used in calculations.

The numerical calculations including integration of the damage evolution equation and failure criterion checking were made in the space of principal values due to the way of the failure criterion and evolution equation formulation. The initial distribution of dimensionless stress tensor principal values corresponding to the ultimate strength σ_u in the virgin state in the ABCDEFGH area is presented in Fig.3a. The identical intensity dashed regions in each element denote stress section explained in Legend. The stress distribution for the assumed damage model characteristic of the metal working at elevated temperature, allows for detecting the regions where the damage nucleation starts after structure is loaded.

The maximum tensile stress appearing in the vicinity of the upper plate edge indicate the first crack location in this area. Very small stress gradient along the AB edge implies an approximately identical speed of damage growth.

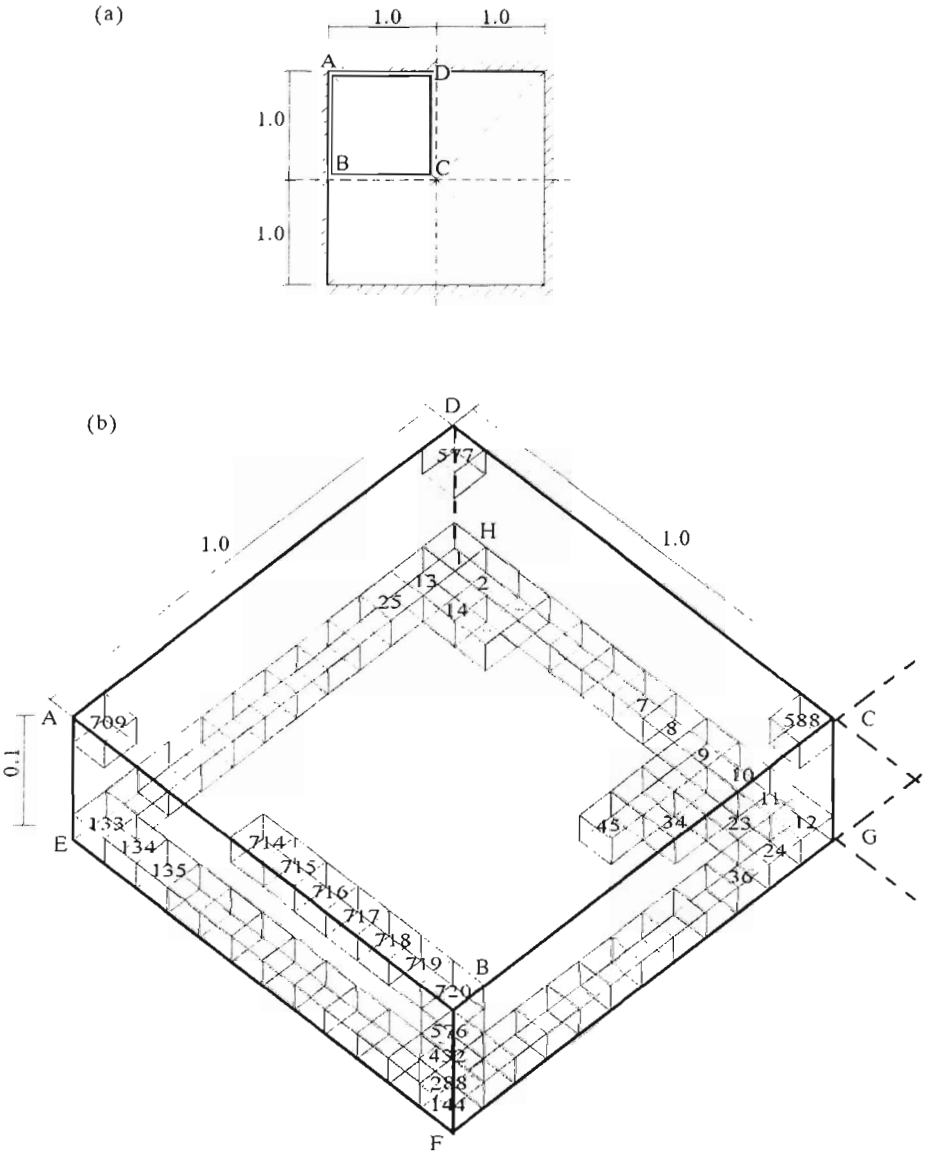
(a)
1.0
1.0
A
D
B
C
1.0
1.0
(b)
D
577
H
1.0
1.0
1
13
2
25
14
7
8
9
10
11
A
709
588
C
1.0
133
134
135
E
714
715
716
717
718
719
B
720
45
34
23
12
24
36
G
576
432
288
144
F

Fig. 2.

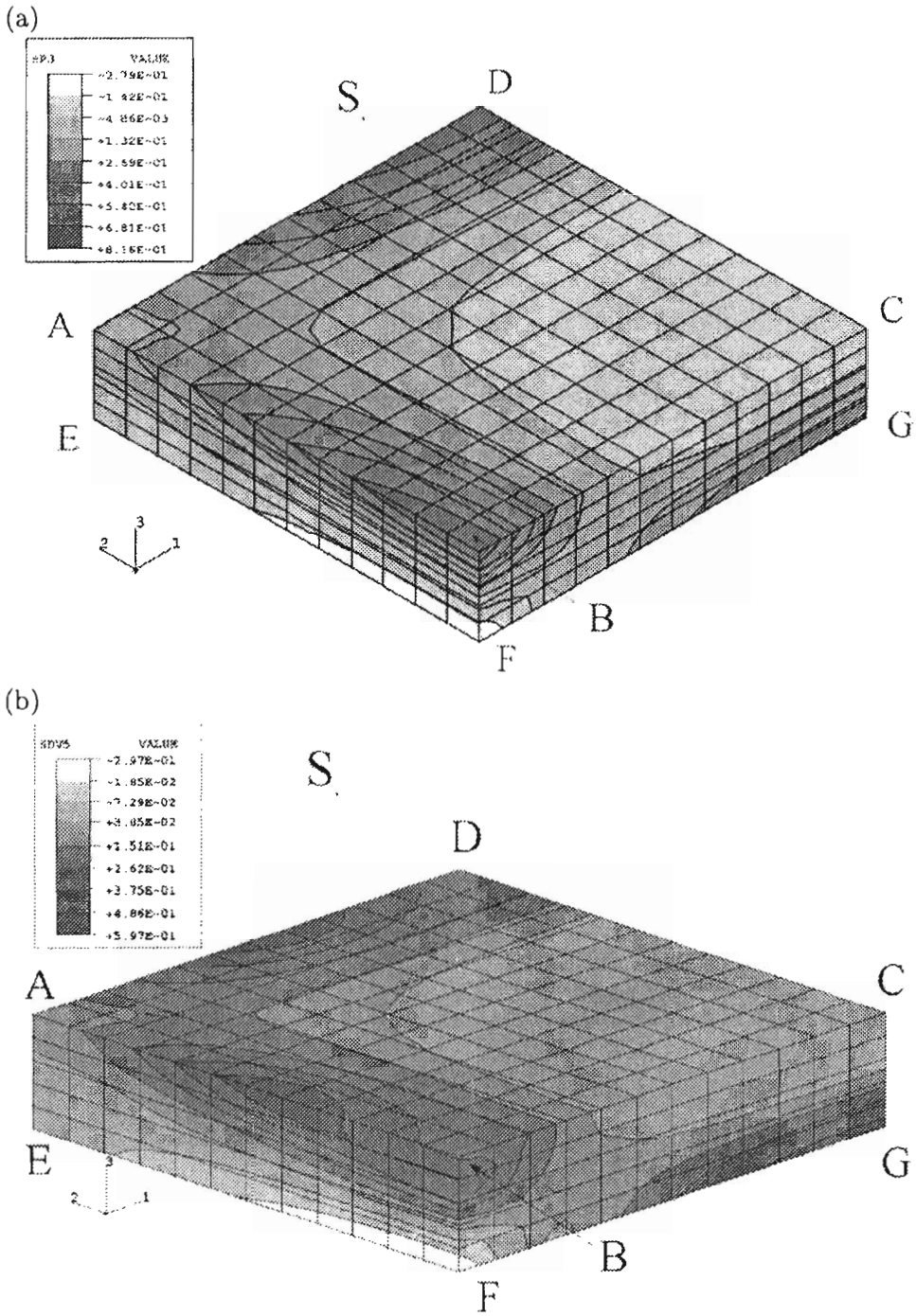

Fig. 3.

Relatively lower intensity of damage evolution in time in the BF direction results from a high stress gradient (narrow regions of compression stresses in the layers $1 \div 3$). Because of symmetry about the ACGE plane, the same course of damage evolution appears at the edges AD and DH. The tensile stresses in vicinity of points C and A of the top layer are related to zero principal values damage tensor. The compressive stresses in the bottom layer, in the vicinity of the geometrical centre of the plate G cause damage evolution which develops less intensively than at the points B and D.

The distribution of dimensionless principal values of the stress tensor at the preceding instant of the first rupture at the points B and D is illustrated in Fig.3b. The damage evolution in the plate leads to a decrease in material stiffness within the damaged regions and to stress redistribution. This effect is included in the constitutive equation, which is a linear combination of the stress and damage tensors. The region of maximum tensile stresses in the cross-section shifts from the points B and D towards the points F and H. At the points located in the vicinity of the centre of the clamped edge AB, a decrease in stresses is insignificant, so they are more exerted than point B. A decrease in plate stiffness causes an expansion of the tensile region in the point G.

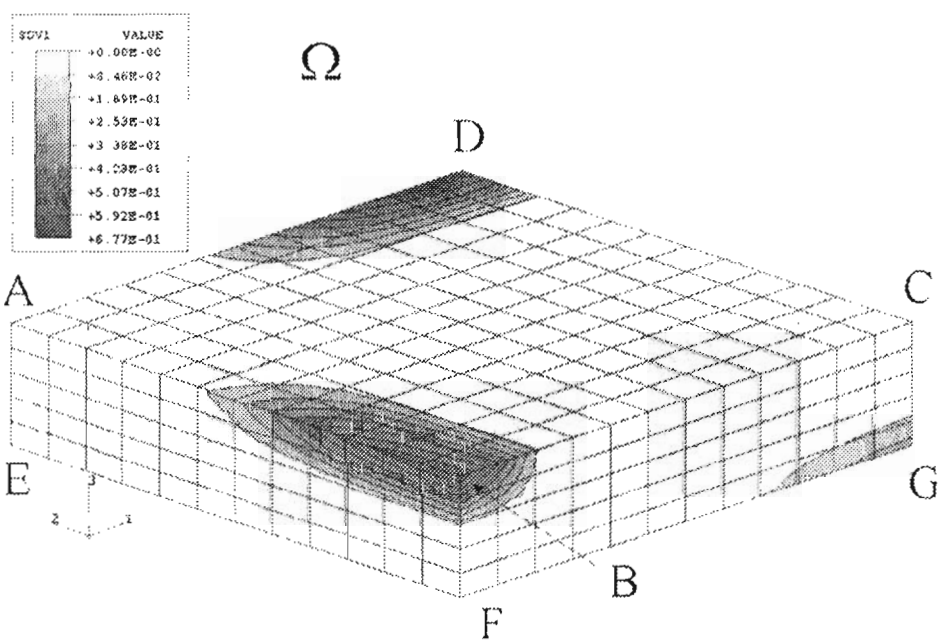

Fig. 4.

The first eigenvalue of the damage tensor Ω_1 distribution in the plate before the first crack occurs ($\bar{t} = 0.98$), is illustrated in Fig.4. We observe the Ω_1 concentration at the centre of clamped edge, i.e. in the elements B and D where the first crack appears.

Damage zone expansion towards the corner A is accompanied by a high gradient of the damage tensor ($\Omega_1 \in (0.0846, 0.677)$) along the edges AB and FB.

For the structures where bending effects predominate, the areas where the first crack appears cover with those of maximum tensile stress. Sample structures for which this dependence does not hold can be shown, e.g. Białkiewicz and Kuna (1996). The authors considered a uniformly loaded plate in a variable boundary strip, where the maximum values of principal tensile stresses in the middle surfaces (shear stresses) were comparable with those in outer surfaces (normal stresses). Under such loading conditions the locations of the first crack are determined by the values of the elastic energy density ($\boldsymbol{M}\boldsymbol{N}^{\top}$ in Eq (2.9)).

The application of solid elements, representing 3D stress state, enable us to model the structure of variable geometry which changes the shape in the damage evolution. Macroscopic cracks in elements lead to reduction of the plate thickness. As a result, the middle plane becomes a three-dimensional surface, which is characteristic of shells. The macrocraks appear in the middle of the top plane edge (vicinity of the points B and D), close to the geometric centre G. Such a geometrical model corresponds to a shallow shell.

The evolution of the principal value of the damage tensor Ω_1 along the clamped edge of the upper plate surface (elements $720 \div 711$) and across the cross-section (elements in the interval $720 \div 144$) are illustrated in Fig.5a and Fig.5b, respectively. The dimensionless scale of the time axis corresponds to the real time of the first cracks. Particular curves are denoted by the O1 symbol, which corresponds to the first value of the damage tensor, afterwards the element number is placed.

The lines drawn in frames represent the history of the damage evolution separately for each element until macrocracks appear. The vertical lines indicate the rupture time in particular elements. Very narrow time span from the moment of cracking represented by line O1_717 in Fig.5a until the elements of the edges AB and AD are damaged, indicates an avalanche character of the crack propagation along the top clamped surface. The macrocracks beginning in the element B, increase loading of all subsequent elements towards the plate corner. It can be seen from the location of the rupture front that the critical damage Ω_1 is decreasing in the process of rupture propagation (Ω_1 is ranging

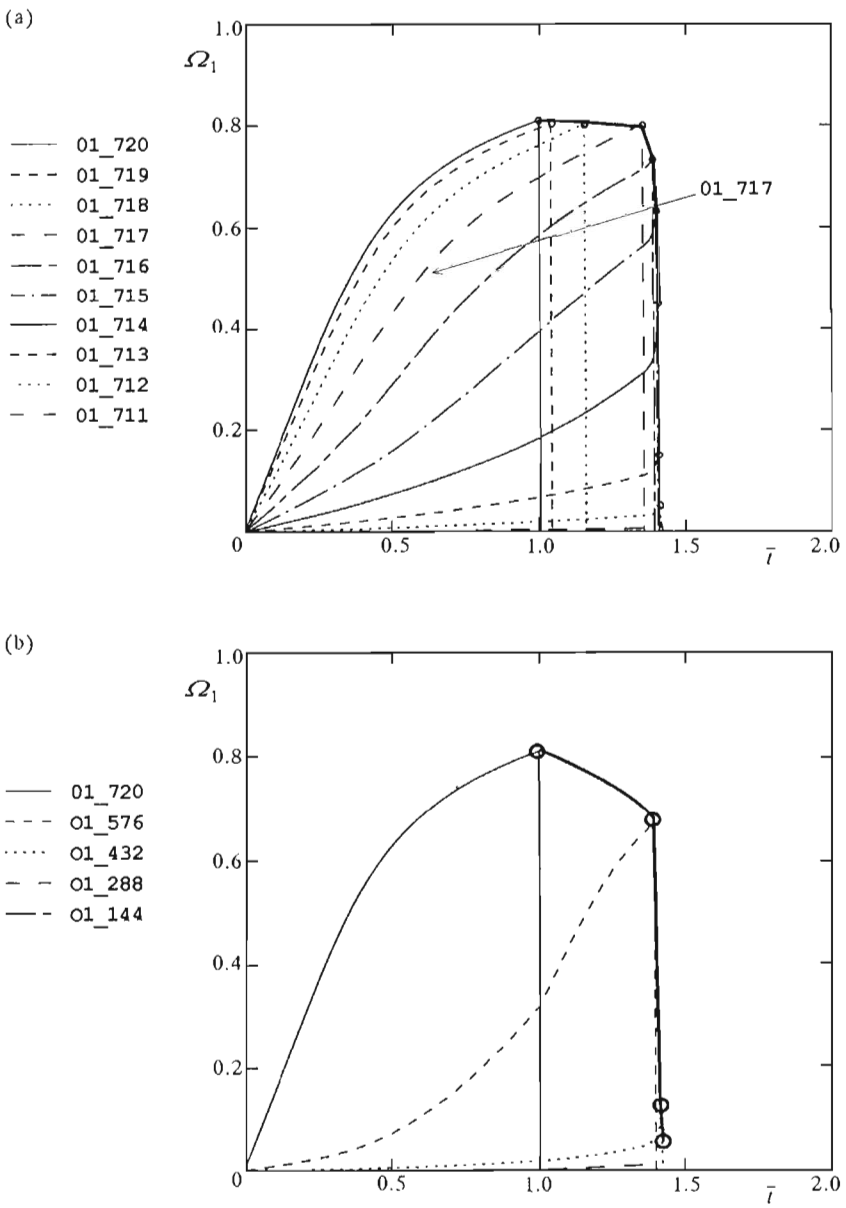
(a)
01_720
01_719
01_718
01_717
01_716
01_715
01_714
01_713
01_712
01_711
Ω_1
1.0
0.8
0.6
0.4
0.2
0
0.5
1.0
1.5
2.0
$\bar{t}$
01_717
(b)
01_720
01_576
01_432
01_288
01_144
Ω_1
1.0
0.8
0.6
0.4
0.2
0
0.5
1.0
1.5
2.0
$\bar{t}$

Fig. 5.

from 0.05 up to 0.81). Experimental investigations conducted for different materials have indicated that the rupture occurs for the values of damage tensor components less than unity, $\Omega \in (0.3, 0.9)$, (cf Litewka, 1985).

Fig.5b illustrates the movement of the damage front in the plate cross-section. In this case the brittle rupture for the assumed division – preceded by a microcrack growth – takes place in the three upper elements of plate only. In the other elements the rupture follows as a consequence of getting to the material ultimate strength in the zone of compressive stresses. A decrease in material stiffness during the damage evolution and decrease in stresses inhibits the process development in the top surface (curve O1_720). In the lower layer, which includes element 576, a rise in damage development rate is observed (curve O1_576) until the first crack in element 720 appears, thus indicating that the layers of lower damage level are loaded. After cracking element 720, the lowest stiffness element 576 reveal and this is why an intensification of damage evolution in element 432 is observed.

The damage process is running in a different way when the constitutive model of linear-elastic undamaged medium is assumed, adopting $\mathbf{D} = \mathbf{0}$ in Eq (2.1). In this model an effect of the damage evolution on the material stiffness is neglected. Until geometrical changes occur (caused by the first crack) the process of damage development is running in the stationary elastic stress field. Cracks appear in the shorter time and smaller degradation of material, (cf Białkiewicz and Mika, 1995). The comparison between solutions for both constitutive models of the elastic medium; i.e., with and without damage, is illustrated in Fig.6.

The dashed lines show the history of the first principal value of the damage tensor for elements of upper clamped plate edge in the case of elastic undamaged material. The dotted lines refer to the results of analogical solution for elastic material with damages. The solid lines in both cases illustrate the history of principal value of the damage tensor on the rupture front. After the rupture of the first four elements (from 720 up to 717) inside the undamage elastic material, due to small degradation at subsequent points, the process of makrocracks forming stops (thick dashed line). Movement of the damage front into element 716 leads to a rapid damage development and when macrocracks occur the damage evolution process has an avalanche character.

Comparison between both the diagrams, in particular the damage front lines, shows that application of the undamaged elastic material model leads to very restrictive design conditions. The time when the first crack occurs for the assumed material and geometrical data regarding the plate is approximately 2.5 times shorter in comparison with the failure time for a structure made

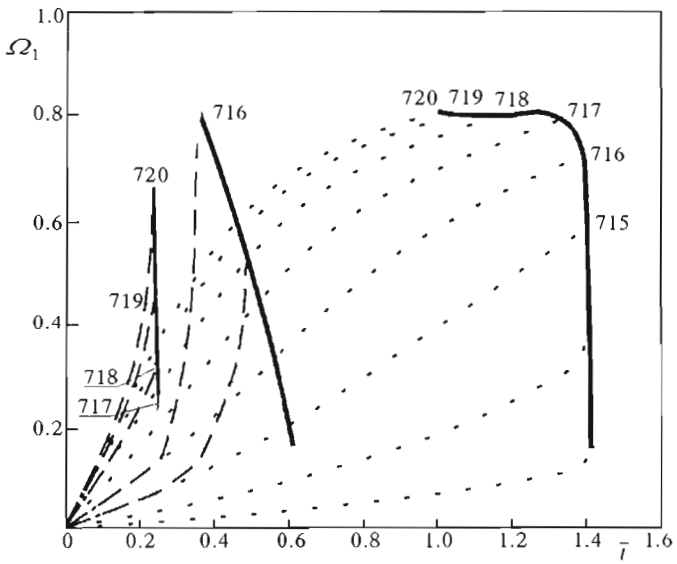
1.0
Ω_1
0.8
0.6
0.4
0.2
0
0.2
0.4
0.6
0.8
1.0
1.2
1.4
1.6
$\bar{t}$
716
720 719 718
717
716
715
720
719
718
717

Fig. 6.

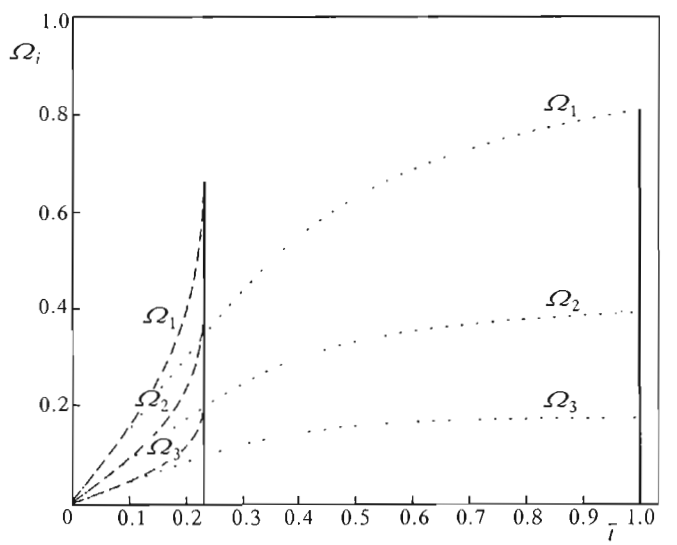
1.0
Ω_i
0.8
0.6
0.4
0.2
0
0.1
0.2
0.3
0.4
0.5
0.6
0.7
0.8
0.9
1.0
$\bar{t}$
Ω_1
Ω_2
Ω_3
Ω_1
Ω_2
Ω_3

Fig. 7.

applying – closer to the real properties – of the elastic material model with time variable stiffness due to damage increase. The assumption of an elastic *in numerical calculations* damaged material made leads to a shorter time of the subsequent cracks formation in comparison to the incubation period of the first cracks than those for elastic undamaged material.

The physical properties of damaged material are related to the property of orthotropy. The evolution of the all three principal components of the damage tensor for both theories in the element with first macroscopic crack 720 is illustrated in Fig.7. The dashed lines illustrate the evolution of the undamaged elastic material, while the dotted lines indicate the history of material with damage. The orthotropy of material is caused by differences between the damage tensor eigenvalues. The divergence of physical properties in each orthotropy direction increases moderately with microcracks evolution.

The presented solutions within the range of crack propagation have been validated by the nominal stress redistribution in the elements of the upper clamped edge (see Fig.8a) and across the plate thickness (see Fig.8b).

The dimensionless principal values of the stress tensor are related to the ultimate strength σ_u of the material. The graphic convention adopted here corresponds to Fig.5a and Fig.5b. The stress redistribution in most exertional elements - due a decrease in material stiffness inhibits the damage process. The stress redistribution in slightly exertional elements reveals a trace character (curves from S1_711 to S1_713), Fig.8a. The vertical lines in both diagrams correspond to the stress clearing on the damage front.

By adopting variable material stiffness in the constitutive description we can illustrate changes of exertion for particular plate layers during movement of the damage front. When time elapses ($\bar{t} = 0.35$) the layer containing element 576 is most exertional – curve S1_576 in Fig.8b. In both lower layers a rise in compressing stresses is observed until ultimate strength is reached.

The material softening process is well illustrated in Fig.9 presenting a relationship between eigenvalues of the damage and stress tensors, respectively, at the element where the first crack occurs. The coupling between the damage and stress tensors in the constitutive equation (2.5) is manifested by the dependence of stress redistribution on damage development. Nonlinearity indicates an acceleration of stress decrease at element 720 in the vicinity of the critical value of the damage tensor. In the case of elastic model which does not involve any stress redistribution, this relationship is linear.

The effective stresses are defined as follows

$$N_i = \frac{S_i}{1 - \Omega_1}$$

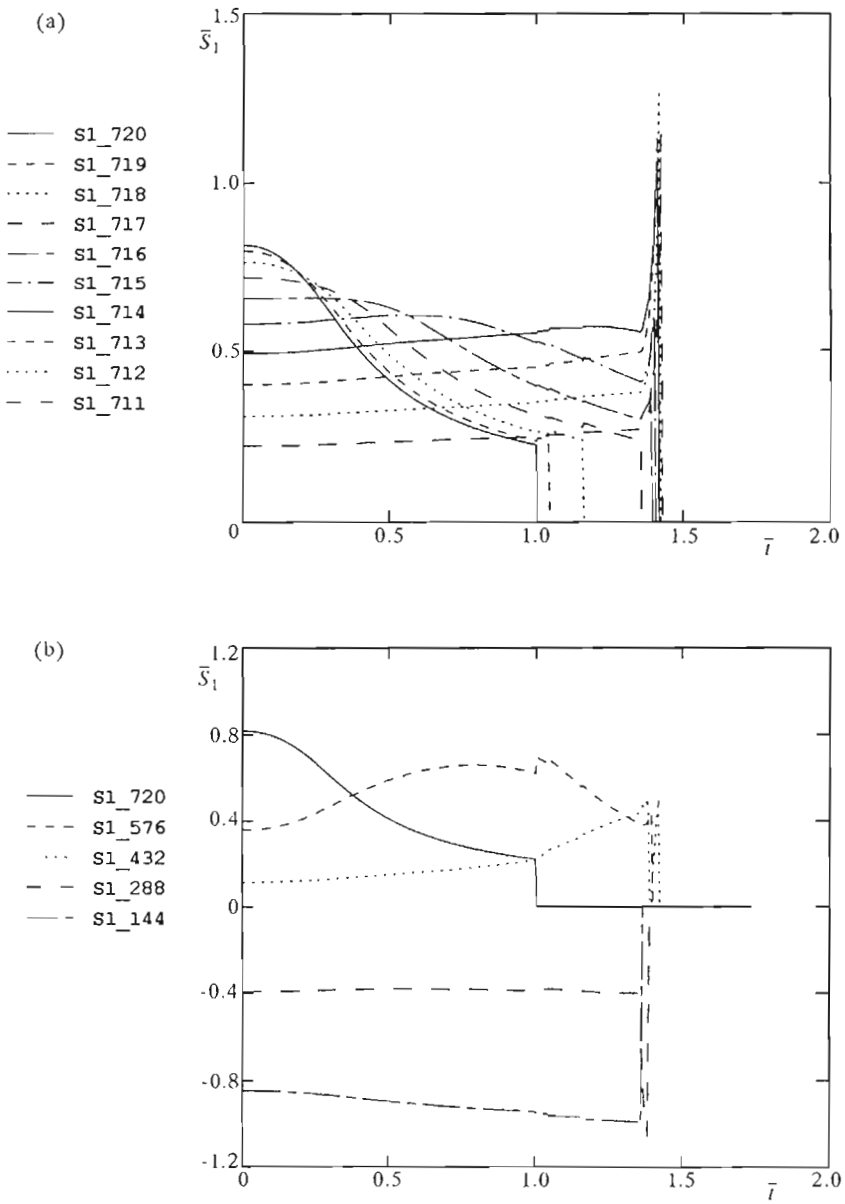
(a)
S1_720
S1_719
S1_718
S1_717
S1_716
S1_715
S1_714
S1_713
S1_712
S1_711
$\bar{S}_1$
1.5
1.0
0.5
0
0.5
1.0
1.5
2.0
$\bar{t}$
(b)
S1_720
S1_576
S1_432
S1_288
S1_144
$\bar{S}_1$
1.2
0.8
0.4
0
-0.4
-0.8
-1.2
0
0.5
1.0
1.5
2.0
$\bar{t}$

Fig. 8.

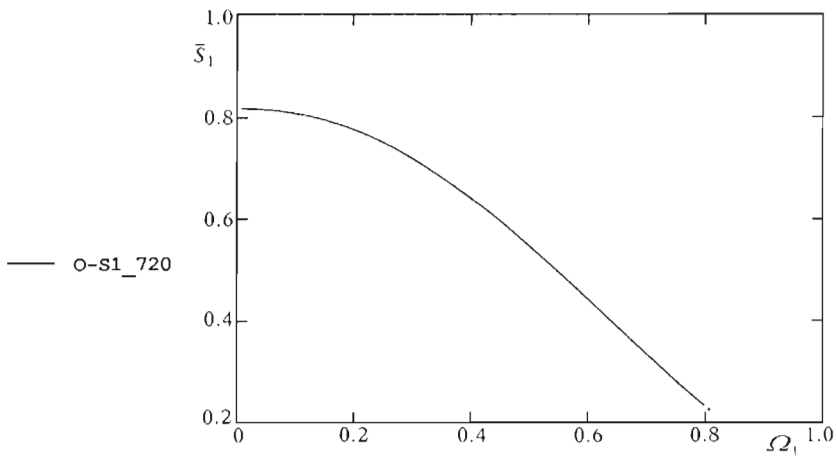

Fig. 9.

where S_i and Ω_i correspond to appropriately normalised eigenvalues of nominal stresses and damage tensor, respectively. The effective stresses make the measure of exertion at a given element objective since they are applied – through the damage tensor – to actual surface of material. N_i increase in time indicates that the process of microcrack nucleation develops; this is why the damage evolution is still observed in elements located along the clamped edge, despite of a considerable stiffness drop, see Fig.10.

A treble increase in the deflection of the plate centre in comparison with instantaneous one in short time scale ($\bar{t} \approx 0.25$, cf Fig.13) is accompanied by intensification of the damage evolution in the vicinity of the geometric centre of the plate in the bottom layer. The elastic stresses are equal here to about 40% of the ultimate stress limit ($\Omega_1 < 0.35$ prior to the crack occurrence in the clamped area), see Fig.11. Until the first crack occurs (see Fig.12) we observe only slight stiffness changes at individual elements, so we can roughly say that damage evolution occurs in the stationary stress field. Movement of the damage front and changes in geometry of the plate cause that the gradient of the stress tensor rapidly increases and the damage condition is fulfilled into elements laying along the axis of symmetry EG of the bottom layer, beginning from the geometric centre of the plate, i.e. element 12. After cracking of the plate centre the damage develops in the form of avalanche. It should be noted that the damage criterion is satisfied when the damage process is poorly (not) developed (for most elements of the bottom layer $\Omega_1 < 0.5$).

Changes of deflection in time for the geometrical centre of the plate are

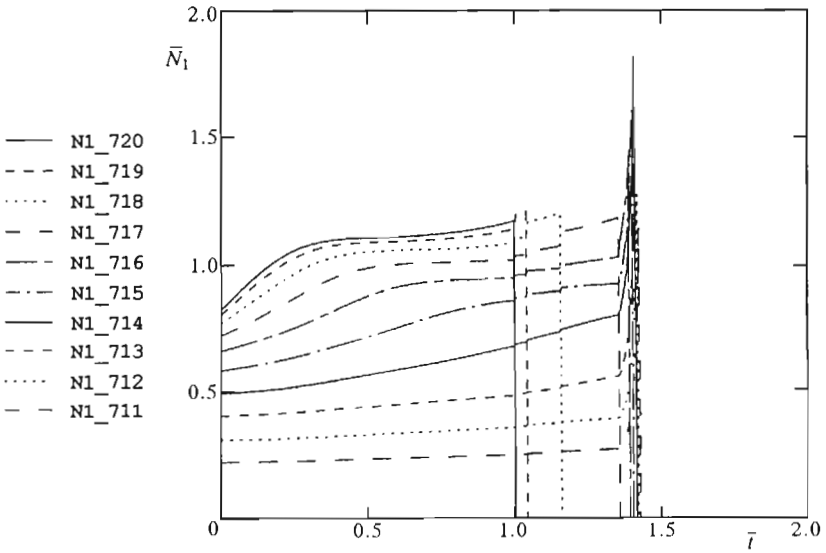
N1_720
N1_719
N1_718
N1_717
N1_716
N1_715
N1_714
N1_713
N1_712
N1_711
$\bar{N}_1$
2.0
1.5
1.0
0.5
0
0.5
1.0
1.5
2.0
$\bar{t}$

Fig. 10.

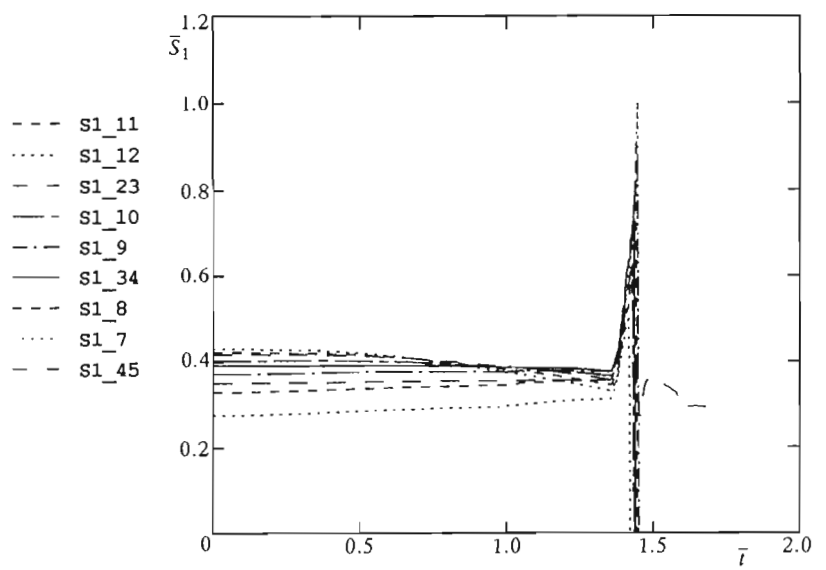
S1_11
S1_12
S1_23
S1_10
S1_9
S1_34
S1_8
S1_7
S1_45
$\bar{S}_1$
1.2
1.0
0.8
0.6
0.4
0.2
0
0.5
1.0
1.5
2.0
$\bar{t}$

Fig. 11.

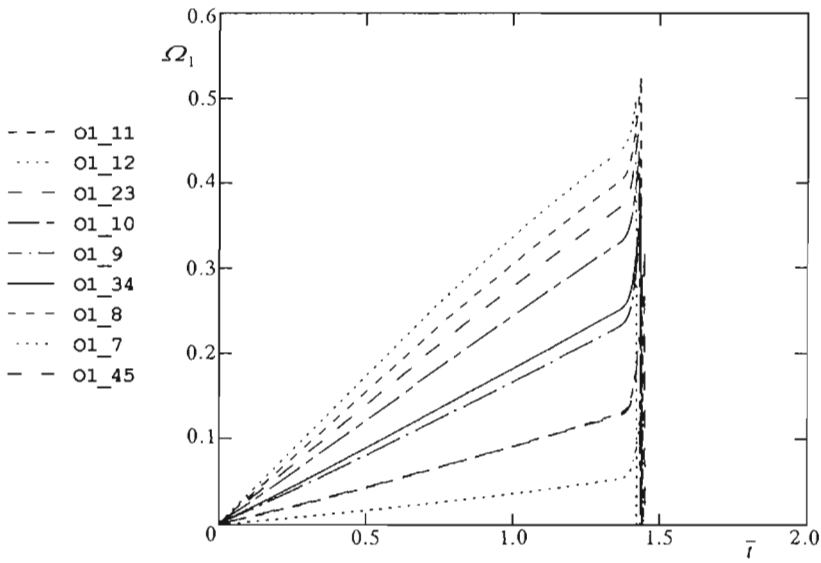
01_11
01_12
01_23
01_10
01_9
01_34
01_8
01_7
01_45
Ω_1
0.6
0.5
0.4
0.3
0.2
0.1
0
0.5
1.0
1.5
2.0
$\bar{t}$

Fig. 12.

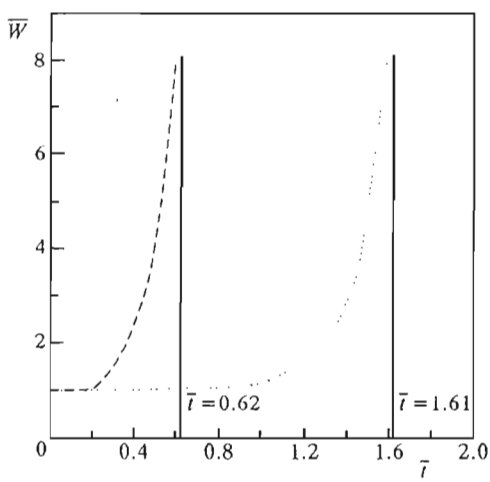
$\overline{W}$
8
6
4
2
0
0.4
0.8
1.2
1.6
2.0
$\bar{t}$
$\bar{t}=0.62$
$\bar{t}=1.61$

Fig. 13.

illustrated in Fig.13. The dimensionless deflection has been related to the instantaneous deflection of the plate. The dotted line shows the deflection increase in time for the elastic model, while the dashed one for the elastic model with damage. The asymptotic behaviour indicates the lifetime of the structure. In the case of elastic material with damage (a dotted line) the first cracks are preceded by a slight deflection increase caused by material softening.

4. Final remarks

The numerical analysis indicates basically a different course of the rupture process, depending on the assumed constitutive model of the material. Application of the constitutive description closer to real properties, which includes changes in material stiffness caused by microcrack development leads to significant elongation of the first crack time. Moreover, the propagation process of the rupture front, in spite of its avalanche character, does not occur in the instantaneous mode. For the elastic material in which softening of material caused by microcrack increase is neglected, the rupture will appear in shorter time and at smaller deterioration of the material (smaller principal values of the damage tensor). Thus we can conclude that the linear-elastic model with damage shall be used for design calculation, whilst the results obtained on the basis of the linear model can be used to estimate the first crack time only.

As a result of microcrack development, the areas of maximum stresses are displaced in the case of material with damage. The adopted form of damage criterion causes – in agreement with the experimental results that the critical values of the damage tensor are less than unity.

The expansion of the damage front and evolution of microcracks lead to replacement of the most exertional plate areas. Changes in damage evolution rate are observed in individual plate layers.

Introduction of the tensor damage measure into mathematical description includes the orthotropic character of the process. The progress of damage development is manifested by the history of effective stresses. Damage evolution proceeds in the stationary stress field in an area surrounding the centre of the plate.

Acknowledgement

The author is grateful to Prof. Jerzy Białkiewicz for formulating the basis of the research and useful suggestions.

This numerical calculations were made on Convex computer in Cyfronet in Cracow and sponsored by the State Committee for Scientific Research (KBN) under grant No. /SPP/PK/073/1996.

References

1. BIAŁKIEWICZ J., KUNA H., 1996, Shear Effect in Rupture Mechanics of Middle-Thick Plates, *Eng. Fract. Mech.*, **64**, 3, 361-370
2. BIAŁKIEWICZ J., MIKA P., 1995, Computer Analysis of Damage Development in Rectangular Plates, *Eng. Trans.*, **43**, 1-2, 71-82
3. CHABOCHE J.L., 1990, On the Description of Damage Induced Anisotropy and Active/Passive Damage Effect, in: *Damage Mechanics in Engineering Materials*, AMD-109, MD-24, J.W. Ju, D. Krajcinovic, H.I. Schreyer, edit. ASME, New York
4. HIBBITT, KARLSSON, SORENSEN, 1997, *ABAQUS Theory and Users Manuals*, Hibbitt, Karlsson and Sorensen, Inc.
5. HSIAO J., FONG M., GIBBONS T.B., 1997, Application of Continuum Damage Mechanics in Multi-Dimensional Creep Failure Analysi – an Efficient Finite Element Solution, *ASME Pressure Vessels Piping Div Publ Pvp.*, **354**, 39-51
6. HUGHES T.J.R., 1987, *The Finite Elemente Method*, Prentice-Hall, Englewood, Cliffs, New York
7. JU J.W., 1991, On Two-Dimensional Self-Consistent Micromechanical Damage Model for Brittle Solids, *Int. J. Solids Structures*, **27**, 2, 227-258
8. KACZANOV L.M., 1958, On Time to Rupture in Creep Conditions (in Russian), *Izv. AN SSSR. OTN*, 26-31
9. KRAJCINOVIC D., 1996, *Damage Mechanics*, Elsevier Science
10. KRAJCINOVIC D., BASISTA M., SUMARAC D., 1994, Basic Principles, in *Damage Mechanics of Composite Materials*, edit. R. Talreja, Elsevier Science B.V.
11. KUNA H., MIKA P., 1996, Structures with Softening Stiffness Induced by Damage, Lightweight Structures in Civil Engineering, *Seminar of IASS Polish Chapter*, Warsaw
12. LITEWKA A, HULT J., 1989, One Parameter CDM Model for Creep Rupture Prediction, *Eur. J. Mech., A/Solids*, **8**, 185-200
13. LITEWKA A., 1985, Effective Material Constants for Orthotropically Damaged Elastic Solid, *Arch. Mech.*, **37**, 631-642
14. MURAKAMI S., HAYAKAWA K., 1997, Thermodynamical Modelling of Elastic-Plastic Damage and Experimental Validation of Damage Potential, *Int. J. Damage Mech.*, **6**, 333-363

15. MURAKAMI S., OHNO N., 1981, A Continuum Theory of Creep and Creep Damage, In: *Creep in Structures*, A.R.S. Ponter and D.R. Hayhurst edit., Springer, Berlin, 422-444
16. MURAKAMI S., SANOMURA Y., 1985, Creep and Creep Damage of Copper Under Multiaxial State of Stress, In: *Plasticity Today*, edit. A. Sawczuk and G. Bianchi, Elsevier Appl. Sci., 535-551
17. PRESS W.H., TEUKOLSKY S.A., VETTERLING W.T., FLANNERY B.P., 1992, *Numerical Recipes: The Art of Scientific Computing*, New York, Cambridge University Press
18. SALEEB A.F., WILT T.E., 1993, Analisis of the Viscoplasitc-Damage Response of Composite Laminates – Continuum Basis and Computational Algorithms, *Int. J. Numer. Methods Eng.*, **36**, 10, 1629-1660
19. VAKULENKO A.A., KACHANOV M.L., 1971, Continuum Theory of Medium with Cracks (In Russian), *Izv. A.N. SSSR, MTT* 159-166
20. VOYIADJIS G., PARK T., 1995, Anisotropic Damage of Fiber Reinforced MMC Using Overall Damage Analysis, *J. of Engineering Mechanics*, **121**, 1209-1217
21. ŻUCHOWSKI R., 1986, Analysis of Failure Processes of Metals Under Conditions For Thermal Fatigue (In Polish), *Sci. Papers. Inst. Mat. Sci and Appl. Mech.*, Wrocław University of Technology, Monograph 18

Współzależność wzrostu uszkodzeń i sztywności materiału w konstrukcjach trójwymiarowych

Streszczenie

Procesy degradacji własności materiału, takich jak wytrzymałość, sztywność i redukcja czasu trwałości są modelowane przez symetryczny tensor uszkodzeń drugiego rzędu wprowadzony do opisu konstytutywnego z zastosowaniem teorii reprezentacji funkcji tensorowych. Wzrost uszkodzeń oraz stan zniszczenia są opisywane przez jednoparametrowe równanie ewolucji oraz trójparametrowe kryterium zniszczenia. W pracy przedstawiono różne formy propagacji frontu zniszczenia w odniesieniu do opisu kostytutywnego. W tym kontekście dokonano porównania rozwiązań otrzymanych z zastosowaniem dwu odmiennych modeli fizycznych: liniowo sprężystego i liniowo sprężystego z uszkodzeniami. W obydwu przypadkach rozważana jest redystrybucja naprężeń spowodowana zmianami geometrycznymi konstrukcji wywołanymi propagacją zarysowań. W obliczeniach numerycznych odwołano się do programu ABAQUS, procedur Rungego-Kutty w całkowaniu równania ewolucji oraz standardowych metod rozkładu macierzy na górno- i dolno-trójkątną, a w zakresie rozwiązywania układu równan algebraicznych – do metody Gaussa.

Manuscript received June 16, 1998; accepted for print November 23, 1998